Supporting Information

Mortise-tenon-like ionic/electronic conductive interface facilitates long-cycle solid-state lithium metal batteries

Guoxiang Zheng,[a] Yifan Jin,[a] Michal Sedlačík,[b] Elif Vargun,[c] Yifan Zhang,[a] Ying He,[a*] Petr Saha,[b] Qilin Cheng [a,b*]

[a] Key Laboratory for Ultrafine Materials of Ministry of Education, Shanghai Engineering Research Center of Hierarchical Nanomaterials, School of Materials Science and Engineering, East China University of Science and Technology, 200237 Shanghai, China. Email: rehey@ecust.edu.cn; chengql@ecust.edu.cn

[b] Centre of Polymer Systems, University Institute, Tomas Bata University in Zlín, Trida T. Bati 5678, 760 01, Zlín, Czech Republic

[c] Chemistry Department, Faculty of Science, Mugla Sitki Kocman University, 48000 Mugla, Turkey

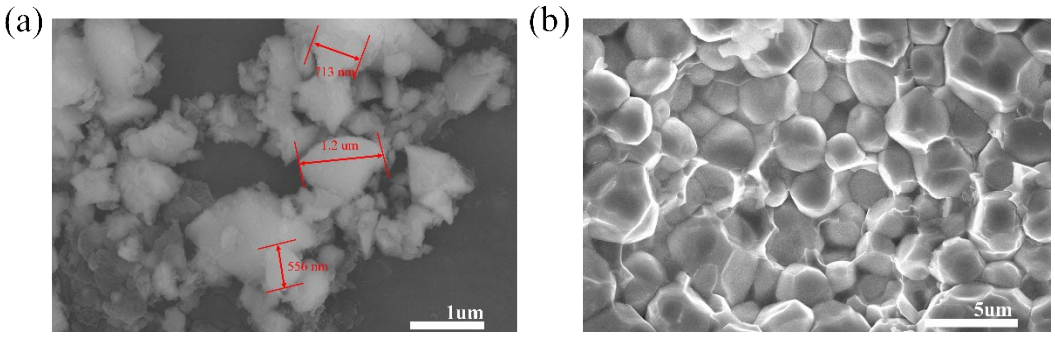

Fig. S1 (a) SEM image of LLZTO powder. (b) Cross-sectional SEM image of LLZTO pellet.

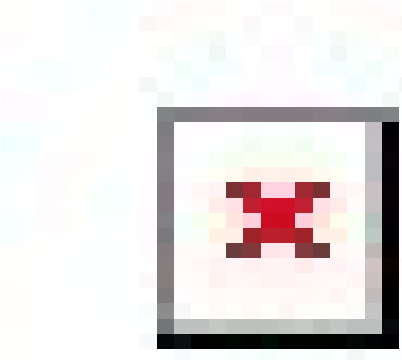

Fig. S2 XRD patterns of standard garnet cubic phase, LLZTO powder and LLZTO pellet.

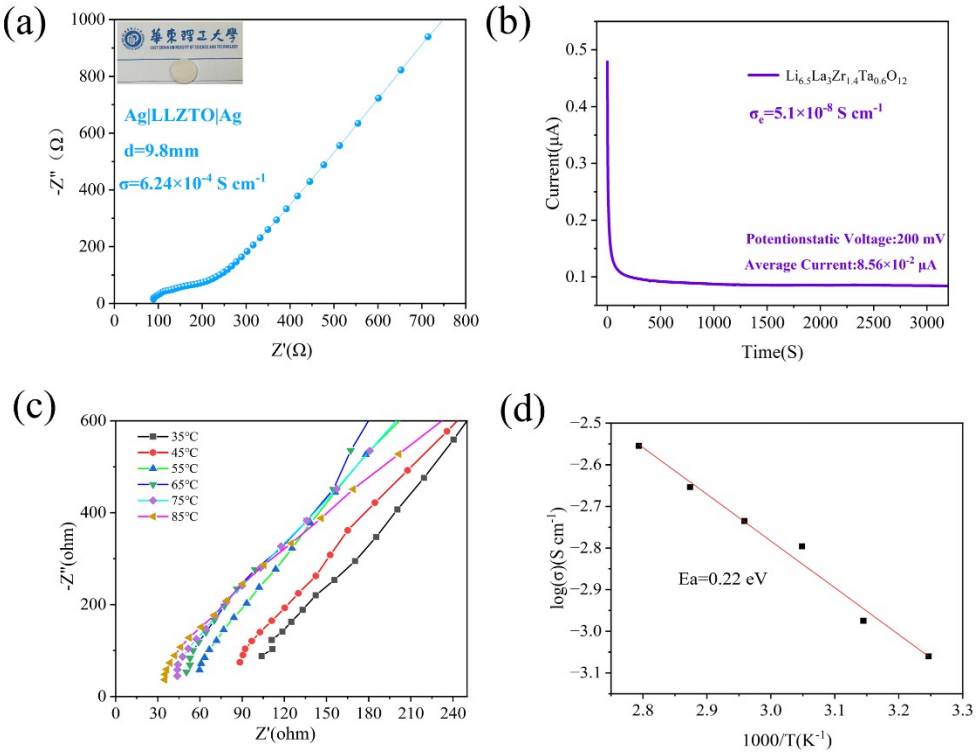

Fig. S3 (a) EIS spectrum of Ag|LLZTO|Ag at room temperature. (b) The DC Polarizatrion of the Ag|LLZTO|Ag at room temperature. (c) EIS spectra of Ag|LLZTO|Ag at different temperature. (d) Arrhenius plots of LLZTO pellet.

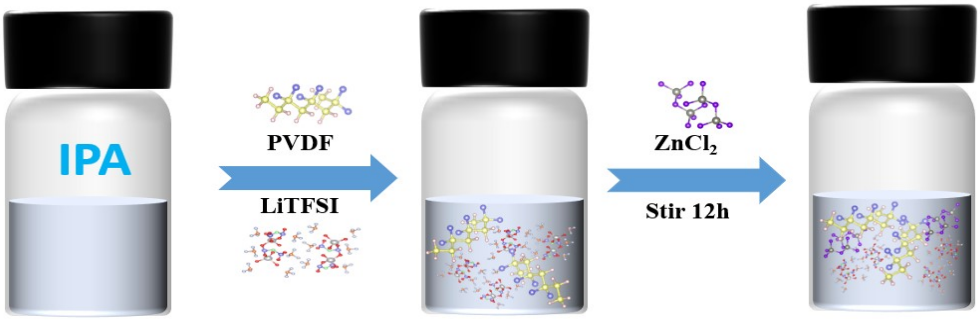

Fig. S4 Schematic diagram of the preparation process for fluorine-containing-$ZnCl_2$ solution.

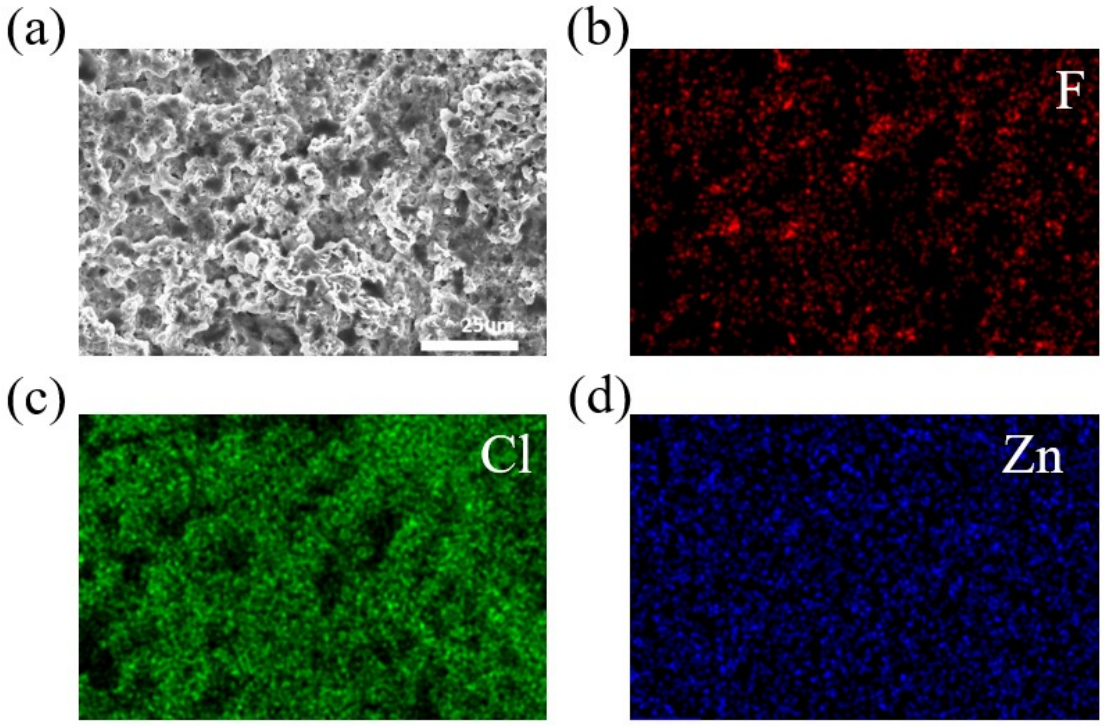

Fig. S5 (a) Surface SEM image of LLZTO after treatment with fluorine-containing-$ZnCl_2$ solution. (b-d) EDS mappings of F, Cl, Zn elements of the modified LLZTO.

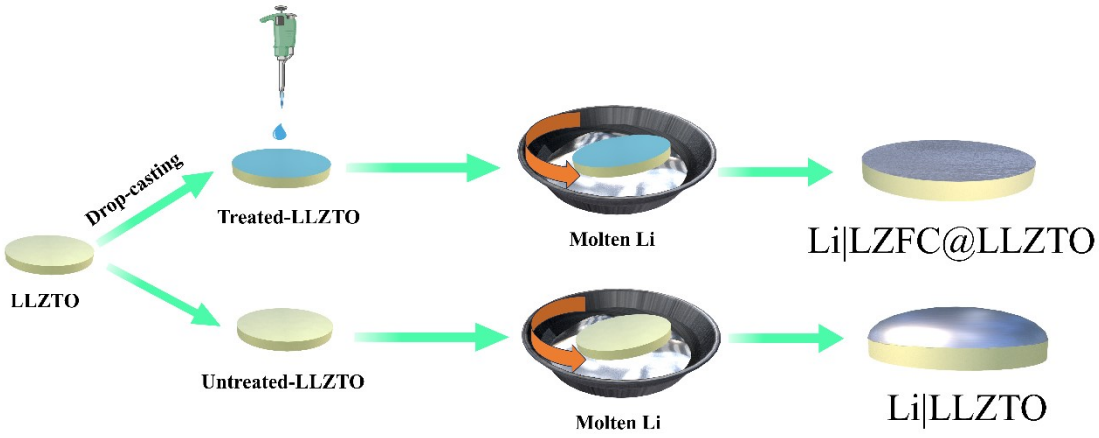

Fig. S6 Schematic diagram of preparation process of the Li/LLZTO and Li/LZFC@LLZTO interface.

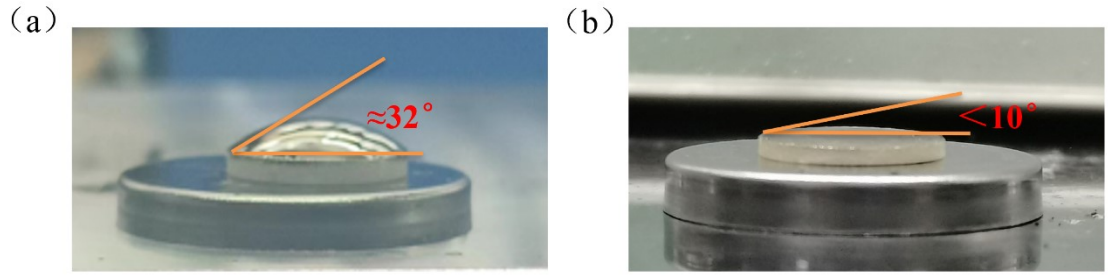

Fig. S7 Comparison of contact angle of (a) Li/LLZTO and (b)Li/LZFC@LLZTO.

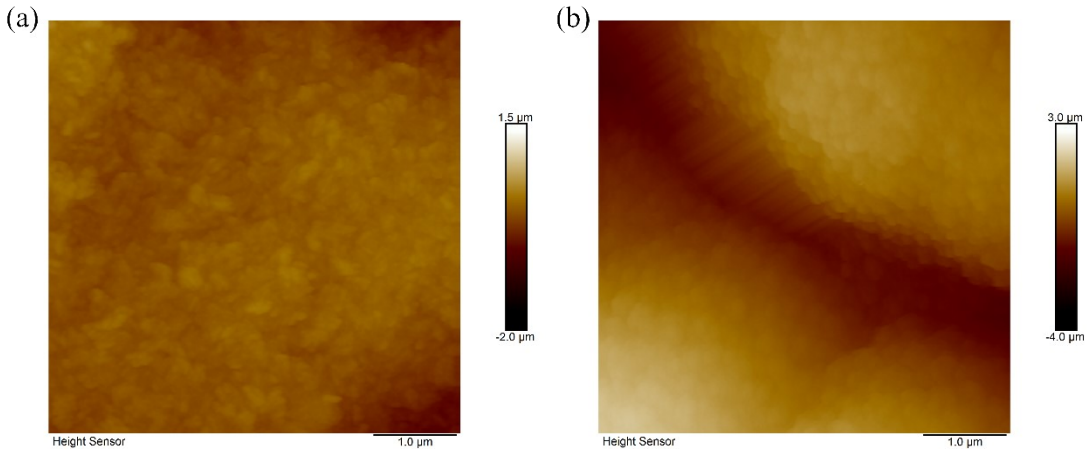

Fig. S8 (a) The 2D surface morphology of LLZTO obtained by AFM. (b) The 2D surface morphology of LZFC@LLZTO after *in situ* lithiation reaction obtained by AFM.

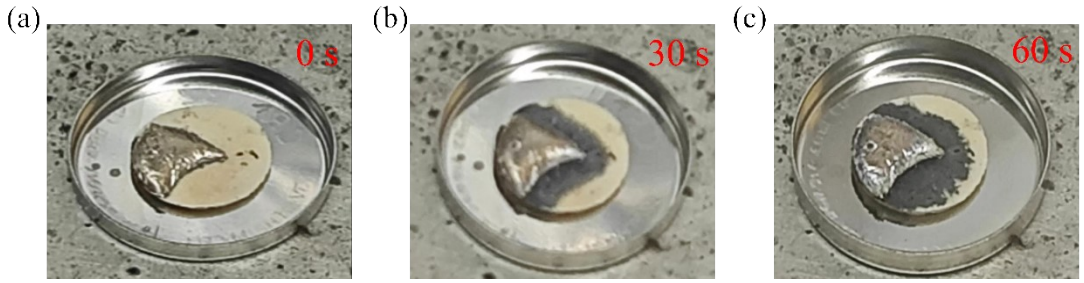

Fig. S9 (a-c) The top side photographs of Li/LZFC@LLZTO after the lithiation reaction with 0 s, 30 s and 60 s.

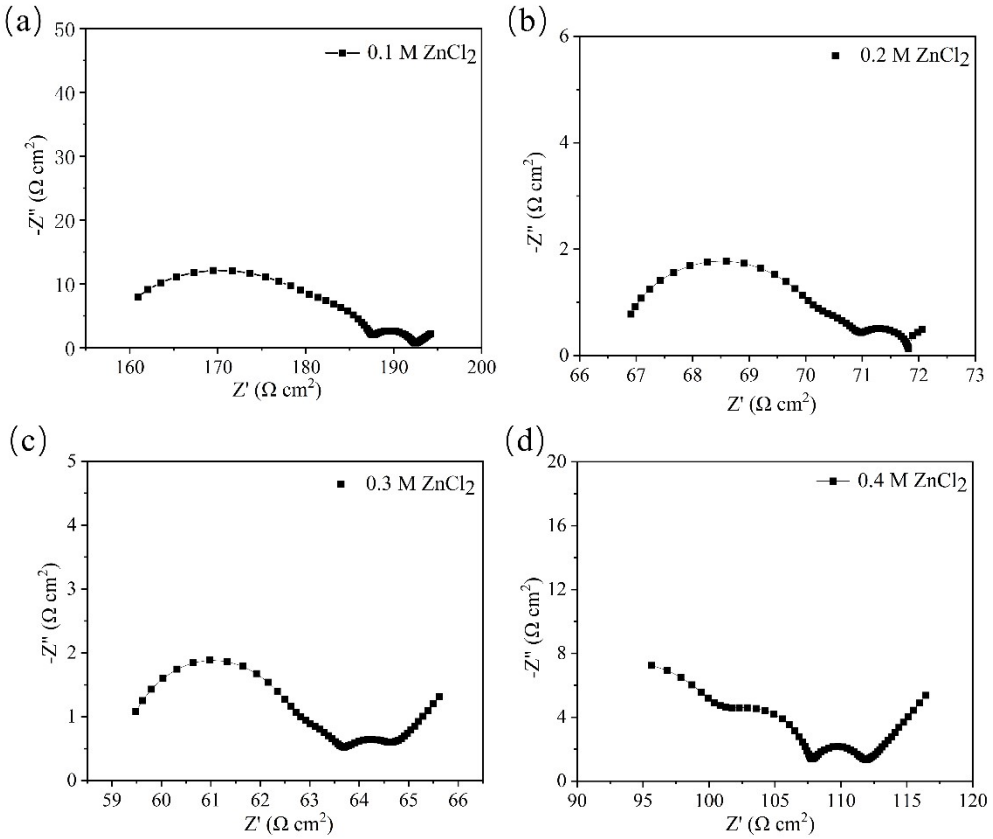

Fig. S10 (a-d) Impedance plots of Li|LZFC@LLZTO|Li with different concentrations of $ZnCl_2$-modified solutions.

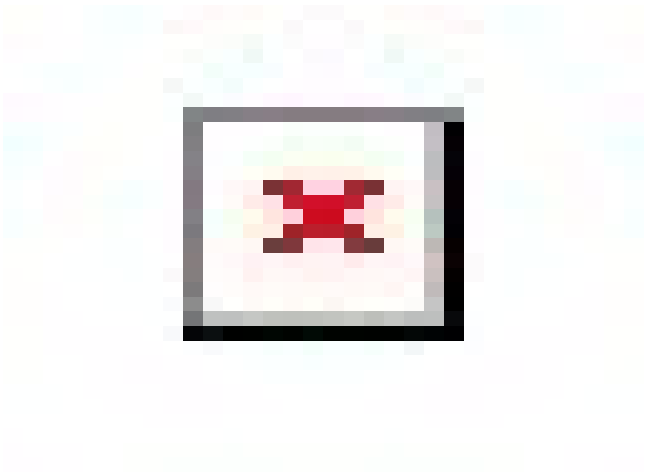

Fig. S11 The CCD of Li|LLZTO|Li cell.

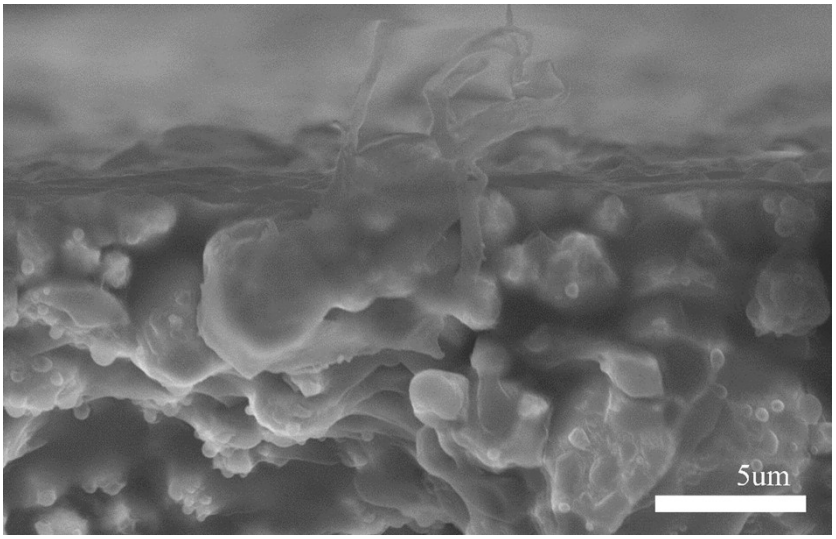

Fig. S12 Cross-section SEM of Li dendrites piercing Li|LLZTO|Li cell.

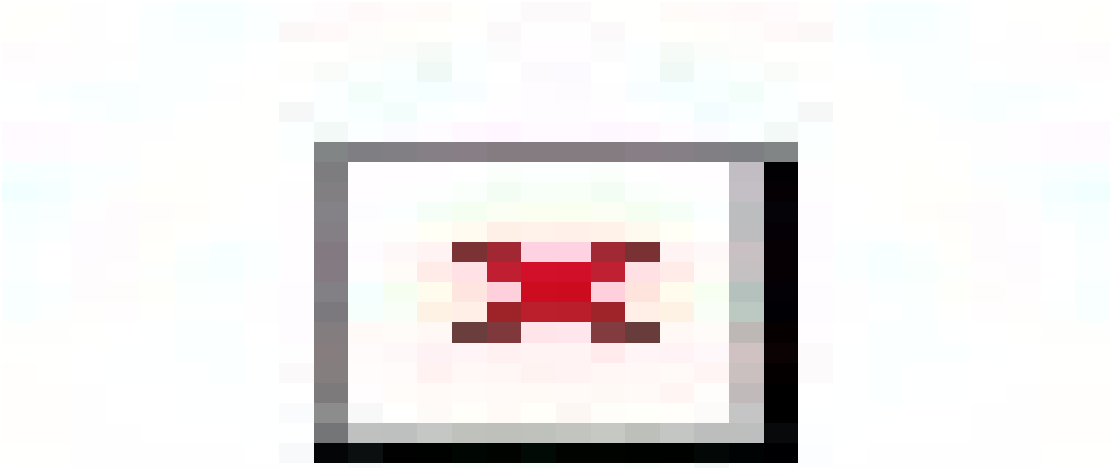

Fig. S13 The constant current cycle comparison between Li|LLZTO|Li and Li|LZFC@LLZTO|Li at 0.2 mA cm^{-2}.

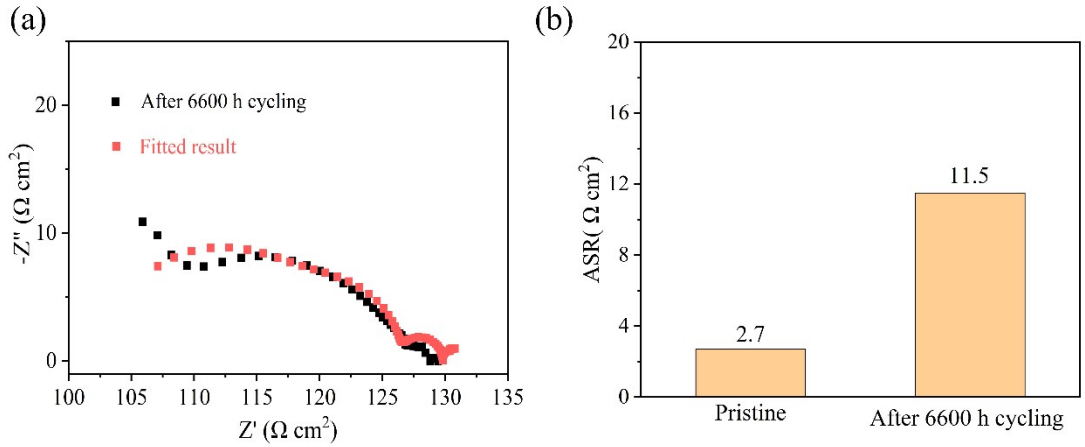

Fig. S14 (a) The EIS spectrum of Li|LZFC@LLZTO|Li after 6600 h cycling. (b) The comparison of ASR between pristine and after 6600 h cycling at 0.2 mA cm^{-2}.

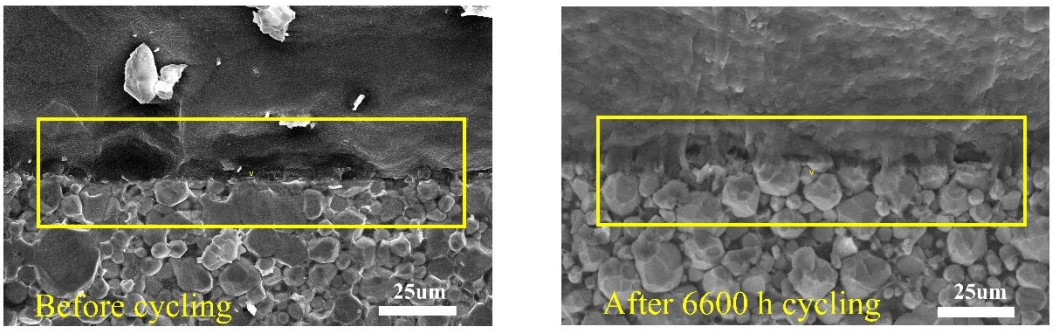

Fig. S15 (a) Cross-section SEM of Li/LZFC@LLZTO before cycling. (b) Cross-section SEM of Li/LZFC@LLZTO after 6600 h cycling at 0.2 mA cm^{-2}.

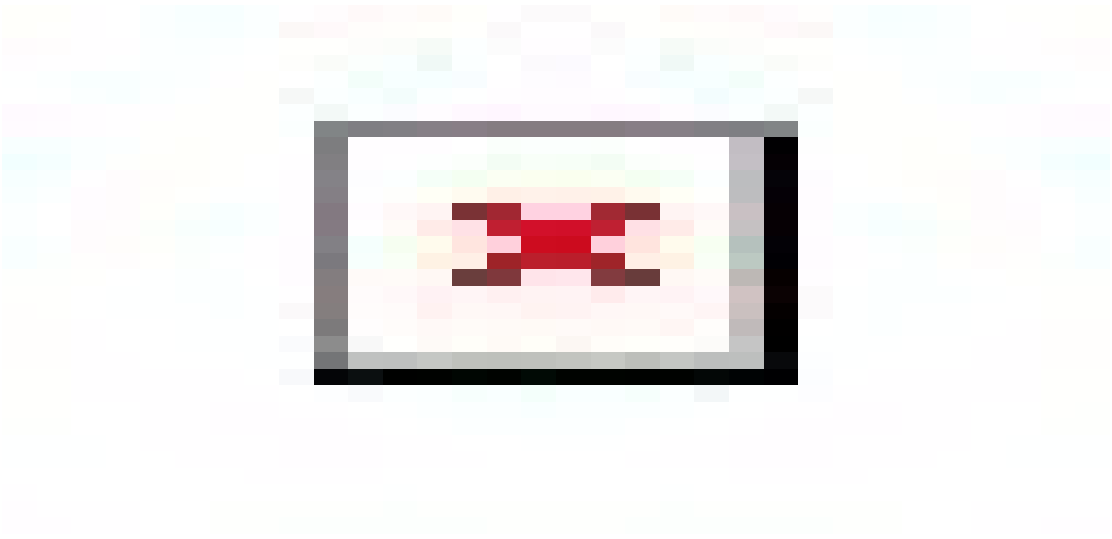

Fig. S16 Long-term galvanostatic cycles of the Li|LZFC@LLZTO|Li at 0.5 mA cm^{-2}.

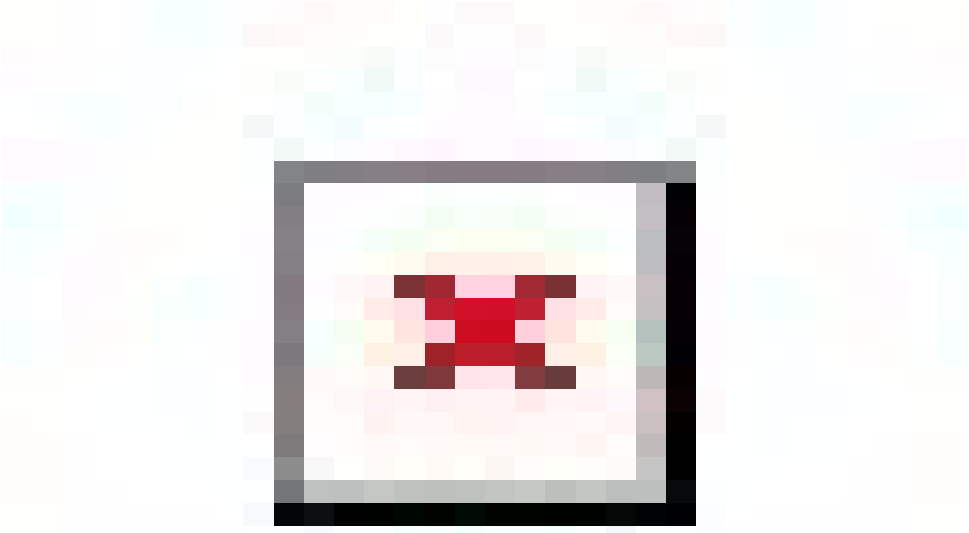

Fig. S17 XPS profile of Zn 2p orbital before and after Li melting.

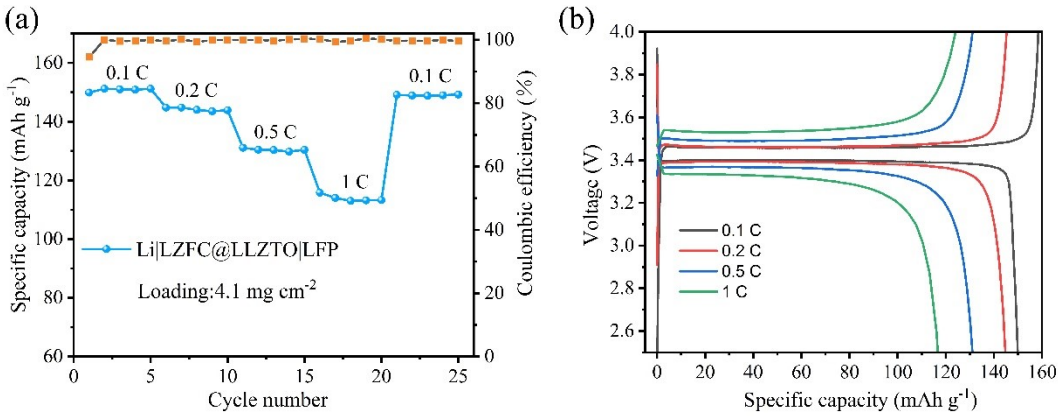

Fig. S18 The rate performance of Li|LZFC@LLZTO|LFP with high load. (b) The voltage capacity curve of Li|LZFC@LLZTO|LFP with high loading.

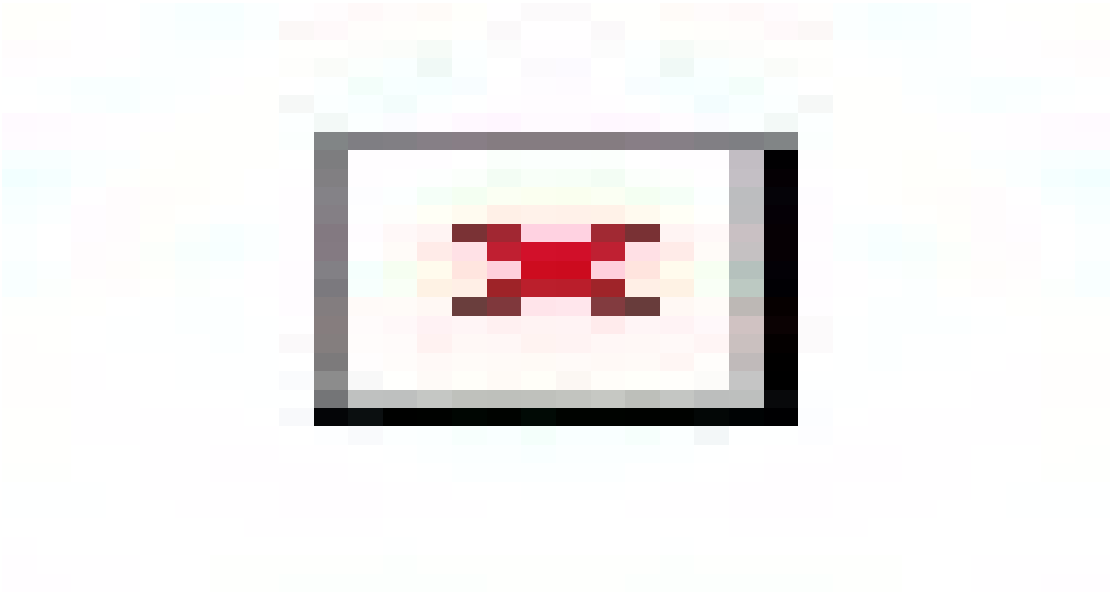

Fig. S19 Cyclic stability of the Li|LLZTO|LFP battery at 0.2 C.

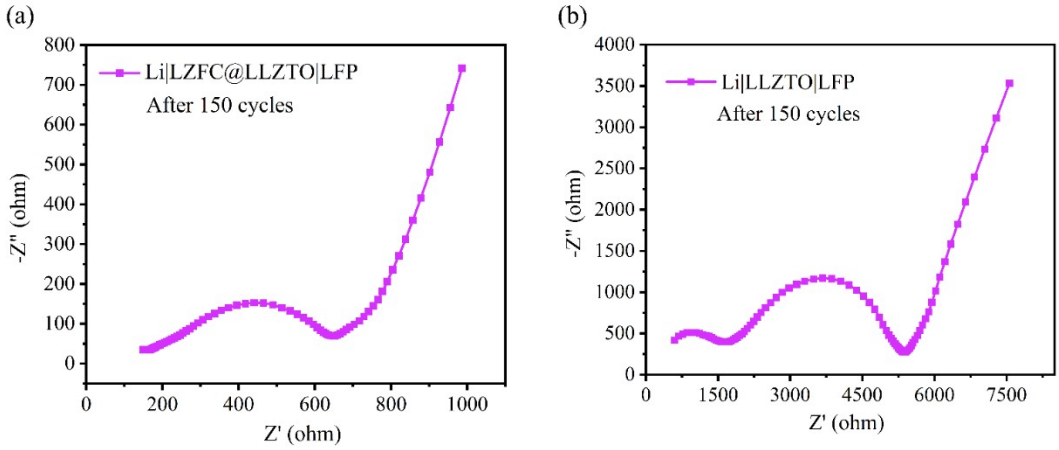

Fig. S20 (a) EIS spectra of Li|LZFC@LLZTO|LFP after 150 cycles. (b) EIS spectra of Li|LLZTO|LFP after 150 cycles.

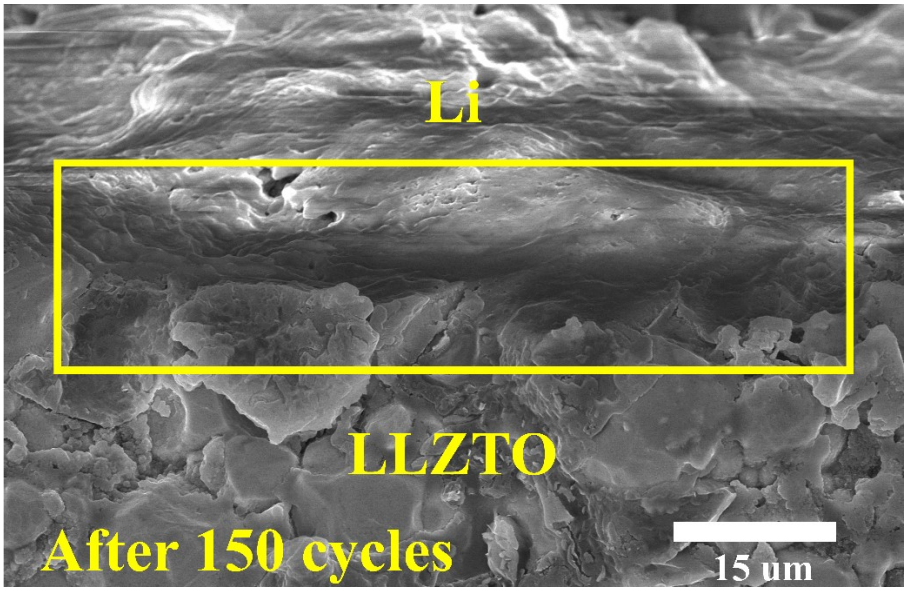

Fig. S21 The cross section SEM of Li/LZFC@LLZTO after 150 cycles of Li|LZFC@LLZTO|LFP.

Table S1 Area specific resistance (ASR), critical current density (CCD) and cycling stability of Li|LZFC@LLZTO|Li compared with recent advanced works.

Interfacial layer	ASR (Ω cm^2)	CCD (mA cm^{-2})	Stability (mA cm^{-2})/h	References
Li-Mg/LiF	25	0.65	0.3/1000	1
Li-BiF_3	7.4	1.1	0.3/850	2
Li–$CaCl_2$	7	1	0.1/1200	3
Li-Li_2Se	5.1	1.4	0.5/350	4
Li-Sr-N	4.5	1.3	0.3/1200	5
Li-SnF_2	11	1.3	0.5/600	6
Li-Sb	4.1	0.64	--	7
Li-LATP	6	1.5	0.3/2500	8
Li-BiOCl	27	1.1	0.5/1000	9
Li-PTLI	33.1	0.71	0.05/1000	10
Li-Al/Si	15	1.2	1/800	11
Li-CoO QDs	12.3	1.1	0.3/1700	12
Li-SnS_2	47	0.5	0.2/1000	13
Li-LTO	25	0.8	0.2/450	14
Li-SnS	5.1	0.9	0.2/1500	15
Li-$LiPO_2F_2$	5.1	1.2	0.6/1500	16
Li-S	12.4	0.7	0.2/1000	17
Li-MXene	5	1.5	0.3/600	18
Li-$InCl_3$	10	0.7	0.2/4000	19
Li-PPA	4	1.8	0.2/2500	20
This Work	**2.7**	**2.1**	**0.2/6600** **0.4/900** **0.5/520**	

Table S2 Liquid electrolyte content, cathode load, areal capacity and liquid/capacity ratios compared with the published literature.

Liquid electrolyte content	Cathode load (mg cm^{-2})	Areal capacity (mAh cm^{-2}) (0.1C)	Liquid/capacity ratios (g/Ah)	References
3uL (3.6 mg)	2.5	0.47	15	21
10uL (12 mg)	3	0.47	29	22
10uL (12 mg)	2.9	0.46	23	11
5uL (6mg)	1.5-2	0.25-0.33	16-21	23
10uL (12 mg)	2	0.29	25	2
8 uL (9.6mg)	2-3	0.3-0.44	19-28	12
3uL (3.6 mg)	1.5	0.23	31	17
3uL (3.6 mg)	1.65	0.26	28	18
10uL (12 mg)	2	0.33	32	25
5uL (6mg)	1-2	0.15-0.3	40-80	14
5uL (6mg)	**4.1**	**0.62**	**10.9**	**This work**

References

1. J. Jiang, Y. Ou, S. Lu, C. Shen, B. Li, X. Liu, Y. Jiang, B. Zhao and J. Zhang, Energy Storage Mater., 2022, **50**, 810-818.
2. Z. Li, X. Jiang, G. Lu, T. Deng, R. Wang, J. Wei, W. Zheng, Z. Yang, D. Tang, Q. Zhao, X. Hu, C. Xu and X. Zhou, Chem. Eng. J., 2023, **465**, 142895
3. Y. K. Liao, R. S. Liu, S. T. Yao and S. F. Hu, ACS Appl. Mater. Interfaces, 2023, **15(49)**, 57828–57834
4. W. Yang, S. Tang, X. Yang, X. Zheng, Y. Wu, C. Zheng, G. Chen, Z. Gong and Y. Yang, ACS Appl. Mater. Interfaces, 2022, **14**, 50710-50717.
5. X. He, X. Ji, B. Zhang, N. D. Rodrigo, S. Hou, K. Gaskell, T. Deng, H. Wan, S. Liu, J. Xu, B. Nan, B. L. Lucht and C. Wang, ACS Energy Lett., 2021, **7**, 131-139.
6. L. Zhang, Q.-K. Meng, X.-P. Feng, M. Shen, Y.-Q. Zhang, Q.-C. Zhuang, R.-G. Zheng, Z.-Y. Wang, Y.-H. Cui, H.-Y. Sun and Y.-G. Liu, Rare Met., 2023, **43**, 575-587.
7. R. Dubey, J. Sastre, C. Cancellieri, F. Okur, A. Forster, L. Pompizii, A. Priebe, Y. E. Romanyuk, L. P. H. Jeurgens, M. V. Kovalenko and K. V. Kravchyk, Adv. Energy Mater., 2021, **11**, 2102086.
8. X. Ye, T. Wang, J. Wen, Q. Yu, Y. Chen, K. Cai and W. Luo, Small Methods, 2024, 2400036.
9. Z. Bi, R. Shi, X. Liu, K. Liu, M. Jia and X. Guo, Adv. Funct. Mater., 2023, **33**, 2307701.
10. X. Wang, Y. Wang, Y. Wu, Y. Fan and Y. Tian, J. Energy Chem., 2023, **78**, 47-55.
11. L. Zhai, K. Yang, F. Jiang, W. Liu, Z. Yan and J. Sun, J. Energy Chem., 2023, **79**, 357-364.
12. G. Lu, Z. Dong, W. Liu, X. Jiang, Z. Yang, Q. Liu, X. Yang, D. Wu, Z. Li, Q. Zhao, X. Hu, C. Xu and F. Pan, Sci. Bull., 2021, **66 (17)**, 1746-1753.
13. B. Zhao, W. Ma, B. Li, X. Hu, S. Lu, X. Liu, Y. Jiang and J. Zhang, Nano Energy, 2022, **91**, 106643.
14. C. Cao, Y. Zhong, B. Chen, R. Cai and Z. Shao, Small Struct., 2023, **4**, 2200374.
15. F. Zhu, W. Deng, B. Zhang, H. Wang, L. Xu, H. Liu, Z. Luo, G. Zou, H. Hou and X. Ji, Nano Energy, 2023, **111**, 2200374.
16. X. Yang, S. Tang, C. Zheng, F. Ren, Y. Huang, X. Fei, W. Yang, S. Pan, Z. Gong and Y. Yang, Adv. Funct. Mater., 2022, **33**, 2209120.
17. J. Wang, S. Zhang, S. Song, J. Liu, Z. Li and H. Zhao, J. Mater. Chem. A, 2023, **11**, 251-258.
18. J. Wen, L. Huang, Y. Huang, W. Luo, H. Huo, Z. Wang, X. Zheng, Z. Wen and Y. Huang, Energy Storage Mater., 2022, **45**, 934-940.
19. J. Leng, H. Liang, H. Wang, Z. Xiao, S. Wang, Z. Zhang and Z. Tang, Nano Energy, 2022, **101**, 107603
20. C. Guo, Y. Shen, P. Mao, K. Liao, M. Du, R. Ran, W. Zhou and Z. Shao, Adv. Funct. Mater., 2022, **33**, 2213443.
21. Zhang, C., Yu, J., Cui, Y. et al. Nat.Commun., 2024, **15**, 5325.
22. Zhai, Lei, Jinhuan Wang, Xiaoyu Zhang, Xunzhu Zhou, Fuyi Jiang, Lin Li, Jianchao Sun, Chem. Sci., 2024, **15** , 7144-7149.
23. Lei Zhang, Qiankun Meng, Yao Dai, Xiangping Feng, Ming Shen, Quanchao Zhuang, Zhicheng Ju, Runguo Zheng, Zhiyuan Wang, Yanhua Cui, Hongyu Sun, Yanguo Liu, Nano Energy, 2023, **113**, 108573.

24. Jie Wang, Saisai Zhang, Hailei Zhao, Jintao Liu, Min-An Yang, Zhaolin Li, Konrad Świerczek, J. Mater. Chem. A, 2024, **12**, 4903-4911.
25. C. Zeng, W. Feng, Y. Shi, X. Zhang, Y. Yang, X. Zheng, Z. Liu, Y. Liu, M. Gao, C. Liang, H. Pan, ACS Appl. Mater. Interfaces,2024, 16 (23), 30462-30470.